Hue University Journal of Science: Natural Science
Vol. 133, No. 1B, 63–69, 2024

pISSN 1859-1388
eISSN 2615-9678

Magneto-optical absorption properties of a Weyl semimetal thin film

Le T. Hoa[1], Le T. T. Phuong[1], Huynh V. Phuc[2]*

[1] Physics Department, University of Education, Hue University, 34 Le Loi St., Hue, Vietnam
[2] Division of Theoretical Physics, Dong Thap University, Cao Lanh, Dong Thap, Vietnam

* Correspondence to Huynh V. Phuc <hvphuc@dthu.edu.vn>
(*Received: 26 July 2023; Revised: 21 August 2023; Accepted: 21 August 2023*)

Abstract. In this study, we investigate the magneto-optical absorption properties of a Weyl semimetal thin film by calculating the magneto-optical absorption coefficients (MOACs) for both intra-band and inter-band transitions. The wave function and energy spectrum were determined using the Hamiltonian minimal model in the presence of magnetic and electric fields. The expressions for the MOACs in both x- and z-directions are obtained using the compact density matrix approach. The numerical results demonstrate that the MOACs are significantly influenced by temperature, carrier concentration, and magnetic and electric fields.

Keywords: Weyl semimetals thin film, Magneto- optical absorption coefficients

1 Introduction

Weyl semimetals (WSMs) exhibit intriguing magneto-optical properties due to the unique electronic structure arising from the presence of Weyl nodes in their band structure. The materials in question have garnered considerable interest in both condensed matter physics and optoelectronics. WSMs display a strong magneto-optical Kerr effect (MOKE) response, which refers to the phenomenon where the polarization of light reflected from or transmitted through the material is altered in the presence of the magnetic field. The unique chirality and Berry curvature associated with the Weyl nodes contribute to the enhanced MOKE signal, making them promising candidates for magneto-optical devices [1]. Furthermore, in WSMs, introducing an external magnetic field induces a remarkable alteration in their electronic characteristics. The giant magnetoresistance in Weyl semimetal thin films opens possibilities for novel magnetic field sensors and memory devices [2]. Moreover, the topological nature of WSMs gives rise to unique magneto-optical phenomena, such as the anomalous Hall effect. These effects are driven by the nontrivial topology of the Weyl nodes and can lead to unusual transport and optical responses that are distinct from those in conventional materials [3].

In recent years, there has been significant research into the magneto-optical properties of two-dimensional layered materials [4-7]. This focus stems from their crucial role in comprehending how semiconductors respond to electromagnetic fields. This study focuses on investigating the magneto-optical absorption properties of a thin film made of WSMs. We achieve this by calculating the magneto-optical absorption coefficients (MOACs), which hold vital significance in comprehending the optoelectronic characteristics and the interplay between light and the distinctive electronic states linked with Weyl

nodes. Additionally, WSMs are categorized as topological materials, distinguished by the existence of Weyl nodes in their electronic band structure. These Weyl nodes serve as sources and sinks of Berry curvature, a fundamental quantity associated with the topological properties of materials. Especially in the presence of a magnetic field, the energy levels of Weyl fermions exhibit Landau quantization, leading to quantized Landau levels (LLs). The MOACs describe the absorption of light when an external magnetic field is applied to the system. The system's Hamiltonian is described using the minimal model, and the corresponding eigenfunctions and eigenvalues are obtained in the presence of magnetic and electric fields. Utilizing density matrix theory, the MOACs for intra- and inter-band transitions are calculated. Section 2 presents the model and theoretical results, while Section 3 discusses the numerical findings. Finally, the conclusion is provided in Section 4.

2 Theory

We introduce a WSMTF with a width in the z direction of L_z. Under the assumption of an infinitely high confinement potential in the z-direction, $V(z)=\infty$, the wave vector k_z undergoes quantization to $k_z=\pm(n_z\pi/L_z)$, where $n_z=1,2,3,...$ is the quantum number in the z-direction. The total wave function can be expressed as $\psi=\psi(x)(e^{ik_y y}/\sqrt{L_y})\phi_{n_z}(z)$, where its component in the z-direction is $\phi_{n_z}(z)=\sqrt{2/L_z}\sin(n_z\pi z/L_z)$. When a magnetic $\vec{B}=(0,0,B)$ and an electric $\vec{E}=(0,0,-E_z)$ field are simultaneously placed in the system, the Hamiltonian of the system can be written as follows [8]

$$H_0=v_F(\pi_x\sigma_x+\pi_y\sigma_y)+T_n\sigma_z, \quad (1)$$

where $v_F=2.5\,\text{eV}\text{Å}/\hbar$ is the Fermi velocity [9], π_x and π_y are the components of the canonical momentum in the x and y-directions, respectively, and $T_n=T_a(k_c^2-k_z^2)-(2T_a/\alpha_c^2)(n+1/2)-\Delta_z$, and σ_x, σ_y, σ_z are the Pauli matrices. Here, $k_c=0.1$ Å^{-1} and $T_a=10$ eV Å^2 are the model parameters [10], $\Delta_z=eE_zL_z$, and $\alpha_c=(\hbar/eB)^{1/2}$ are the magnetic length. The energy level and wave function corresponding to the Hamiltonian (1) are given as follows for the states with the LL index $n\neq 0$

$$E_{n,p}^{n_z}=p\sqrt{n(\hbar\omega_c)^2+T_a^2}=pE_n^{n_z},\ \omega_c=v_F\sqrt{2}/\alpha_c, \quad (2)$$

$$\psi(x)=\psi_{n,p}^{n_z}(x)=\begin{bmatrix}A_{n,p}^{n_z}\phi_{n-1}(x)\\ ipB_{n,p}^{n_z}\phi_n(x)\end{bmatrix}, \quad (3)$$

where $\phi_n(x)$ is the oscillator function and

$$A_{n,p}^{n_z}=\sqrt{\frac{pE_n^{n_z}+T_n}{2pE_n^{n_z}}},\ B_{n,p}^{n_z}=\sqrt{\frac{pE_n^{n_z}-T_n}{2pE_n^{n_z}}}. \quad (4)$$

For the state with $n=0$, we have $E_0^{n_z}=-T_0$, and $\psi_0^{n_z}=(0,\phi_0)^T$, with T being the transpose.

The susceptibility of a WSMTF, when irradiated by an incident electromagnetic wave with energy $\hbar\omega$, can be expressed as follows [6, 11-13]

$$\varepsilon_0\chi_{\mu\nu}(\omega)=\frac{1}{V}\sum_{\xi',\xi}\sum_{k_y'k_y}\frac{(f_\xi-f_{\xi'})(d_{\xi',\xi}^{\mu})^*d_{\xi',\xi}^{\nu}}{\Delta E_{\xi',\xi}-\hbar\omega-i\hbar\Gamma_0}, \quad (5)$$

where V is the system volume, ε_0 is the vacuum permittivity, $\xi\equiv\{n,p,n_z\}$, $(\mu,\nu)=(x,y,z)$, f_ξ is the Fermi-Dirac distribution function for the $|\xi\rangle$ state, $\Delta E_{\xi',\xi}=E_{\xi'}-E_\xi$ is the transition energy, and the phenomenological damping rate is chosen to be $\Gamma_0=1$ meV. The dipole element in the μ direction is given as follows

$$d_{\xi',\xi}^{\mu}=-\frac{e}{\Delta E_{\xi',\xi}}\delta_{k_y',k_y}\delta_{n_z',n_z}\langle\xi'|[H_0,\mu]|\xi\rangle. \quad (6)$$

pISSN 1859-1388
eISSN 2615-9678

After having the susceptibility expression, the absorption coefficient (AC) is obtained as follows [4, 5, 14]

$$\alpha_{\mu\nu}(\omega)=\omega\sqrt{\frac{\mu_0}{\varepsilon_0 n_r^2}}\,\mathrm{Im}\left[\varepsilon_0\chi_{\mu\nu}(\omega)\right], \quad (7)$$

where μ_0 is the vacuum magnetic permeability and $n_r=6$ is the refractive index of the WSMTF [15]. In this paper, we are interested in the $\alpha_{xx}(\omega)$ and $\alpha_{zz}(\omega)$ components of the ACs. Using the commutative systems $[H_0,x]=-i\hbar v_F\sigma_x$ and $[H_0,z]=2ik_zT_a\sigma_z$, the dipole elements in equation (6) can be obtained as follows

$$d^{x}_{\xi',\xi}=\frac{e\hbar v_F}{\Delta E_{\xi',\xi}}\left[pA^{n_z}_{n',p'}B^{n_z}_{n,p}\delta_{n',n+1}-p'B^{n_z}_{n',p'}A^{n_z}_{n,p}\delta_{n',n-1}\right], \quad (8)$$

$$d^{z}_{\xi',\xi}=\frac{2\pi ien_zT_a}{\Delta E_{\xi',\xi}L_z}\left(A^{n_z}_{n',p'}A^{n}_{n,p}-pp'B^{n_z}_{n',p'}B^{n}_{n,p}\right)\delta_{n',n}. \quad (9)$$

Then, by inserting them into equation (7), we can obtain the expressions for $\alpha_{xx}(\omega)$ and $\alpha_{zz}(\omega)$.

3 Numerical results

In this section, we show our numerical calculations for the $\alpha_{xx}(\omega)$ and $\alpha_{zz}(\omega)$ components of the absorption coefficient. Our results are categorized into two main parts based on the doping level. The first part pertains to the undoped intrinsic WSMTF, where the chemical potential (CP) μ_p resides within the bandgap. The second part relates to the doped scenario, where the CP is located in the conduction band.

a. Undoped WSMTF

In this case, the carrier concentration is zero ($n_c=0$), and the μ_p is located inside the gap. Therefore, the absorption spectrum is solely formed by inter-band transitions, wherein an electron in the valence band absorbs the energy of the photon and moves to the conduction band.

In Fig. 1, we show the $\alpha_{xx}(\omega)$ and $\alpha_{zz}(\omega)$ versus photon energy, where the impact of the electric field is denoted by a dimensionless parameter $\gamma=\Delta_z/(T_ak_c^2)$. We can see that both

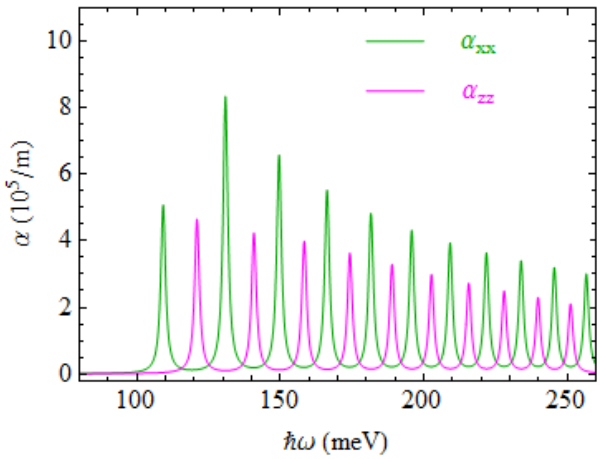

Fig. 1. MOACs versus photon energy at $n_c=0, B=8$ T, $T=0$ K, and $\gamma=0.5$

$\alpha_{xx}(\omega)$ and $\alpha_{zz}(\omega)$ display a series of peaks. The peaks in $\alpha_{xx}(\omega)$ are generated by a mixture of a transition pair $L_{-n(-n-1)}\to L_{n+1(n)}$, except for the first peak, which is formed by only one transition $L_0\to L_1$. Meanwhile, all the peaks in $\alpha_{zz}(\omega)$ are formed by the transition $L_{-n}\to L_n$. This accounts for an intriguing finding wherein the height of the initial peak is lower than the subsequent one. This result is also observed in TMDCs [16] and in topologically insulating thin films [6]. Furthermore, we observe that, due to the larger transition energy in the *z*-direction compared to the *x*-direction, the absorption spectrum of $\alpha_{zz}(\omega)$ is positioned to the right of the absorption spectrum of $\alpha_{xx}(\omega)$. From Fig. 1, we also notice that as the LL index increases, the height of the peaks exhibits a decrease. This outcome can be understood as follows: When the n (LL index) increases, the transition energy also increases, conducing to a decrease in the dipole element (see Eq. (6)). As both $\alpha_{xx}(\omega)$ and $\alpha_{zz}(\omega)$ are proportional to the dipole element, the height of the absorption coefficient diminishes with

increasing n. Furthermore, we observe that as the LL index increases, the spacing between peaks decreases in both $\alpha_{xx}(\omega)$ and $\alpha_{zz}(\omega)$, meaning the peaks become progressively closer to each other. This is the result of the fact that the spacing between two adjacent peaks, $\Delta\omega_n = E_{n+2} - E_n$, is found to decrease with increasing n.

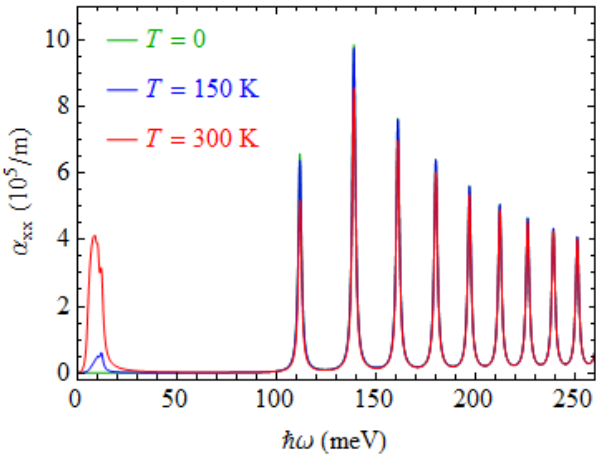

Fig. 2. The $\alpha_{xx}(\omega)$ versus photon energy for different temperatures at $n_c = 0, B = 8$ T, and $\gamma = 0.5$

Fig. 2 displays the influence of temperature on $\alpha_{xx}(\omega)$. Since temperature does not influence the absorbed photon energy, the position of the absorption peaks remains unchanged. However, as the temperature rises, thermal excitation allows for certain intraband transitions to occur, leading to the emergence of intraband transition peaks.

Notably, higher temperatures correspond to increased absorption peaks.

The impact of the electric field, represented by the dimensionless parameter $\gamma = \Delta_z / (T_a k_c^2)$, on the $\alpha_{xx}(\omega)$ is depicted in Fig. 3. It is evident that as the electric field strength increases, the transition energy decreases, resulting in a red-shift feature in the absorption spectrum.

Figure 4 demonstrates the impact of the magnetic field on the absorption spectrum. It is evident that as the B increases, the absorption exhibits a blue-shift behavior due to the rise of the cyclotron energy with the magnetic field's increase.

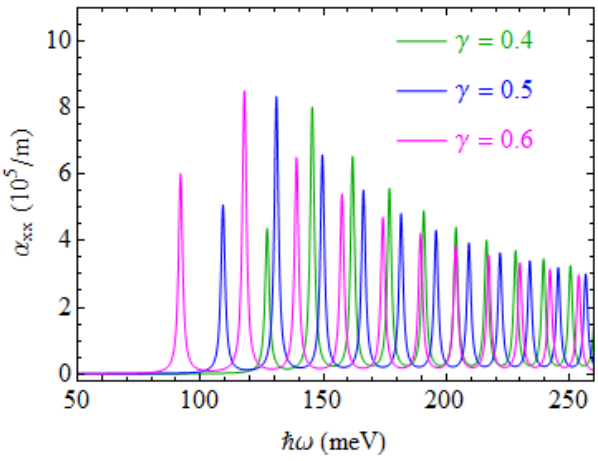

Fig. 3. The $\alpha_{xx}(\omega)$ versus photon energy for different values of electric field at $n_c = 0, B = 8$ T, and $T = 0$

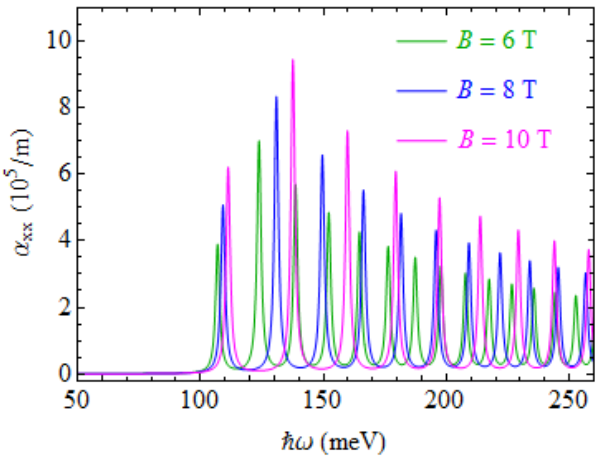

Fig. 4. The $\alpha_{xx}(\omega)$ versus photon energy for different magnetic fields at $n_c = 0$, $\gamma = 0.5$, and $T = 0$

b. Doped WSMTF

Now, we shift our focus to the doped WSMTF scenario, where $n_c \neq 0$ is present, and as a result, the CP is located within the conduction band. Consequently, both intra- and interband transitions become possible.

Figure 5 shows the effect of temperature on the $\alpha_{xx}(\omega)$. Here, we re-choose the value of $\Gamma_0 = 0.1$ meV for clearer peak observation and denote $n_0 = 5\times10^{23} m^{-3}$. With $n_c = n_0$, the CP μ_p

pISSN 1859-1388
eISSN 2615-9678

lies between the LLs L_3 and L_4. In this case, at the zero temperature (T = 0), only the intraband transition $L_3 \to L_4$ is permissible, and all other transitions are prohibited. The value of absorbed photon energy in this case is $\hbar\omega_{3,4} = E_{4,1} - E_{3,1} = 7.95$ meV. As the temperature increases, certain LLs positioned below the CP (L_0, L_1, L_2, and L_3) undergo thermal depopulation; as a result, some of the lower Landau levels are no longer fully occupied. This leads to the possibility of electrons from these lower levels transitioning to fill the vacant states, thereby giving rise to new intraband transitions. Such transitions can be observed as $L_2 \to L_3$ at $\hbar\omega_{2,3} = 8.76$ meV and $L_1 \to L_2$ at $\hbar\omega_{1,2} = 7.95$ meV. Note that the transition $L_0 \to L_1$ at $\hbar\omega_{0,1} = 11.79$ meV is also formed in this case. However, its magnitude is too small to be observed in Fig. 5. Simultaneously, the LLs located above the CP ($n \geq 4$) are not entirely empty because of thermal effects. With the increase in temperature, the thermal excitation effect becomes stronger, leading to a greater number of LLs above the CP becoming occupied. These electrons can now transit to higher LLs, leading to the generation of extra peaks corresponding to the $L_n \to L_{n+1}$ transitions, where $n \geq 4$. The

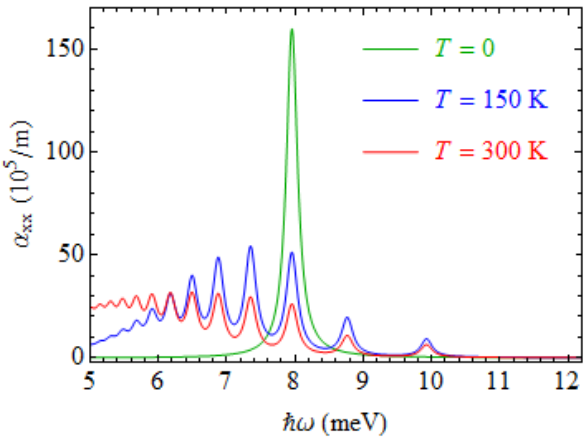

Fig. 5. The $\alpha_{xx}(\omega)$ for intra-band transitions versus photon energy for different temperatures at $n_c = n_0$, $B = 8$ T, $\Gamma_0 = 0.1$ meV, and $\gamma = 0.5$

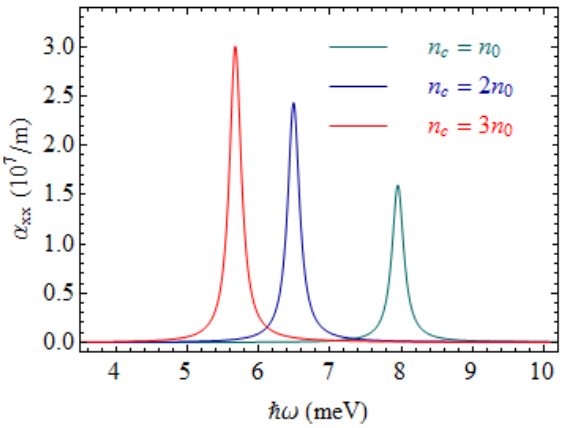

Fig. 6. The $\alpha_{xx}(\omega)$ for intra-band transitions versus photon energy for different values of n_c at $T = 0$, $B = 8$ T, $\Gamma_0 = 0.1$ meV, and $\gamma = 0.5$

supplementary peaks are positioned at lower energies relative to the main peak ($L_3 \to L_4$). A comparable result is also observed in thin films of graphene [7] and topological insulators [6].

Figure 6 shows the effect of carrier concentration on the $\alpha_{xx}(\omega)$ for intra-band transitions at $T = 0$, $B = 8$ T, $\Gamma_0 = 0.1$ meV, and $\gamma = 0.5$. It is noted that at T = 0, there is only one intra-band transition, where its Landau levels are adjacent above and below the CP. Furthermore, the position of the CP is directly proportional to the carrier concentration. The higher the carrier concentration, the higher the position of the CP, leading to a larger separation between LLs. Specifically, for carrier concentrations of $n_c = n_0$, $2n_0$, and $3n_0$, the CP lies between the LLs L_3 and L_4, respectively, corresponding to the transitions $L_n \to L_{n+1}$ with (n = 3, 6, 7). The values of the absorbed photon energy corresponding to these transitions are 7.95 (6.49, 5.67) meV. Consequently, we observe that as n_c increases, the peak shifts towards the lower energies, resulting in a red-shift.

In Fig. 7, we show the $\alpha_{xx}(\omega)$ for inter-band transitions versus the photon energy for different values of temperature. Unlike in the undoped situation, where all the inter-band transitions are allowed (see Fig. 2), here, in the doped case, only

DOI: 10.26459/hueunijns.v133i1B.7263

the transitions where the final LLs are above the CP will occur. With $n_c = n_0$, the CP lies between L_3 and L_4. Hence, at T = 0, the first transition is $L_{-3} \to L_4$, while the other ones whose final LLs have $n \le 3$ are blocked. When the T increases, thermal excitation leads to a situation where the LLs below the CP are not fully filled. Electrons from the lower LLs can now move to fill these partially empty levels, resulting in the formation of new absorption peaks. These new peaks are observed in both cases at T = 150 K and T = 300 K, as shown in Fig. 7.

In Fig. 8, we show the $\alpha_{xx}(\omega)$ for inter-band transitions versus photon energy for different values of carrier concentration at $T = 0$, $B = 8$ T, $\Gamma_0 = 1$ meV, and $\gamma = 0.5$. As illustrated in Fig. 7, at T = 0, the inter-band transitions start to happen when the final LL is adjacent to the CP. Notably, the position of the CP is directly proportional to n_c, such that increasing n_c pushes the CP to a higher energy position. Consequently, the first shift occurs at a higher-order LL (larger n), resulting in the absorbed photon's energy having a larger value. This explanation accounts for the findings presented in Fig. 8, where an increase in n_c leads to a shift of the absorption spectrum towards higher energy regions (blue-shift line).

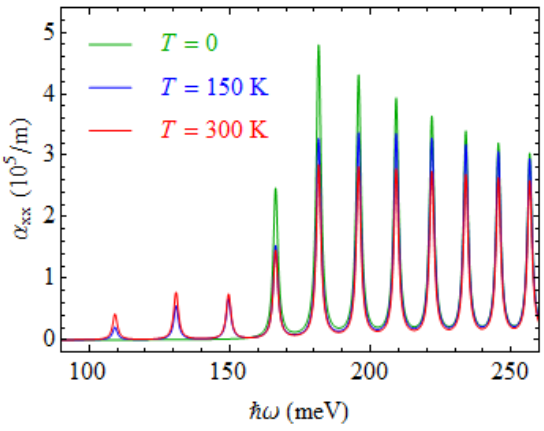

Fig. 7. The $\alpha_{xx}(\omega)$ for inter-band transitions versus photon energy for different temperatures at $n_c = n_0$, $B = 8$ T, $\Gamma_0 = 1$ meV, and $\gamma = 0.5$

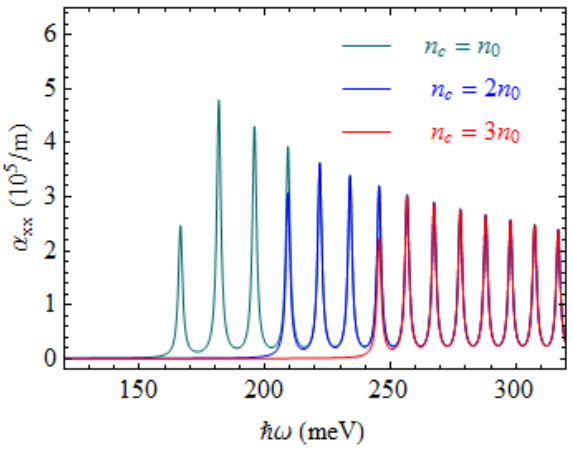

Fig. 8. The $\alpha_{xx}(\omega)$ for inter-band transitions versus photon energy for different values of carrier concentration at $T = 0$, $B = 8$ T, $\Gamma_0 = 1$ meV, and $\gamma = 0.5$

4 Conclusion

We have investigated the MOACs for both x and z-directions in a WSMTF for both undoped and doped cases. Both $\alpha_{xx}(\omega)$ and $\alpha_{zz}(\omega)$ components of the absorption coefficient exhibit a series of peaks, but $\alpha_{zz}(\omega)$ does not display the half-peak feature observed in $\alpha_{xx}(\omega)$. In the undoped case, only intra-band transitions are allowed at T = 0, while both intra-band and inter-band transitions occur in the doped case. The influence of temperature, carrier concentration, magnetic field, and electric field on the MOACs has also been studied, revealing new transitions due to thermal excitation in both intra-band and inter-band transitions. This study contributes to our understanding of fundamental physics and highlights the potential for advanced optoelectronic devices and quantum technologies in WSMs. Further research in this area holds promise for unveiling new practical and transformative applications.

pISSN 1859-1388
eISSN 2615-9678

Acknowledgement

Le T. Hoa was funded by the Master, PhD Scholarship Programme of Vingroup Innovation Foundation (VINIF), code VINIF.2022.TS047.

References

1. Trépanier O, Duchesne RN, Boudreault JJ, Côté R. Magneto-optical Kerr effect in Weyl semimetals with broken inversion and time-reversal symmetries. Physical Review B. 2022;106(12):125104.
2. Liang T, Gibson Q, Ali MN, Liu M, Cava RJ, Ong NP. Ultrahigh mobility and giant magnetoresistance in the Dirac semimetal Cd3As2. Nature Materials. 2015;14(3):280-4.
3. Yang X, Zhou X, Feng W, Yao Y. Strong magneto-optical effect and anomalous transport in the two-dimensional van der Waals magnets Fen GeTe2 (n=3, 4, 5). Physical Review B. 2021;104(10):104427.
4. Bich TN, Phuc HV, Dinh L. Magneto-optical absorption coefficients in monolayer MoSe2. Hue University Journal of Science: Natural Science. 2021;130(1B):21-6.
5. Nguyen CV, Hieu NN, Duque CA, Khoa DQ, Hieu NV, Tung LV, Phuc HV. Linear and nonlinear magneto-optical properties of monolayer phosphorene. J Appl Phys. 2017;121(4):045107.
6. Hieu NV, Kubakaddi SS, Hieu NN, Phuc HV. Magneto-optical absorption properties of topological insulator thin films. Journal of Physics: Condensed Matter. 2022;34(30):305702.
7. Scharf B, Perebeinos V, Fabian J, Žutić I. Magneto-optical conductivity of graphene on polar substrates. Physical Review B. 2013;88(12):125429.
8. Hoa LT, Phuong LTT, Kubakaddi SS, Hieu NN, Phuc HV. Landau levels and magneto-optical responses in Weyl semimetal quantum wells in a non-uniform magnetic field. Physical Review B. 2022;106(7):075412.
9. Lu H-Z, Zhang S-B, Shen S-Q. High-field magnetoconductivity of topological semimetals with short-range potential. Physical Review B. 2015;92(4):045203.
10. Zhang S-B, Zhou J. Quantum oscillations in acoustic phonons in Weyl semimetals. Physical Review B. 2020;101(8):085202.
11. Yao X, Belyanin A. Giant Optical Nonlinearity of Graphene in a Strong Magnetic Field. Physical Review Letters. 2012;108(25):255503.
12. Huong PT, Muoi D, Bich TN, Phuc HV, Duque CA, Nguyen PTN, Nguyen CV, Hieu NN, Hoa LT. Intra- and inter-band magneto-optical absorption in monolayer WS2. Physica E: Low-dimensional Systems and Nanostructures. 2020;124:114315.
13. Yao X, Belyanin A. Nonlinear optics of graphene in a strong magnetic field. Journal of Physics: Condensed Matter. 2013;25(5):054203.
14. Tung LV, Bau NQ, Bich TN, Vinh PT, Phuc HV. Linear and Nonlinear Magneto-optical Absorption Coefficients and Refractive Index Changes in Wse2 Monolayer. VNU Journal of Science: Mathematics - Physics. 2021;37(4):59-67.
15. Buckeridge J, Jevdokimovs D, Catlow CRA, Sokol AA. Bulk electronic, elastic, structural, and dielectric properties of the Weyl semimetal TaAs. Physical Review B. 2016;93(12):125205.
16. Catarina G, Have J, Fernández-Rossier J, Peres NMR. Optical orientation with linearly polarized light in transition metal dichalcogenides. Physical Review B. 2019;99(12):125405.